

# The pit-craters and pit-crater-filling lavas of Masaya volcano

Andrew J. L. Harris

Received: 2 December 2007 / Accepted: 30 July 2008 / Published online: 11 September 2008  
© Springer-Verlag 2008

**Abstract** Lava flowing into a pit crater will become entrapped to form an inactive lava lake. At Masaya volcano (Nicaragua) pit filling lavas are exposed in the walls of Nindiri, Santiago and San Pedro pits. Mapping of these lavas shows that fill can involve emplacement of both 'a'a and pahoehoe, with single fill units ranging in thickness from 2 to 22 m. Thick units with columnar joints were emplaced as simple inactive lava lakes during high effusion rate episodes. Sequences of thinner units, which can form pit floor shields or compound lakes, were emplaced at lower effusion rates. Lava withdrawal caused unsupported sections of three 20-m-thick units to subside, resulting in unit flexure and faulting, and viscous peeling features reveal that subsidence occurred while at least one unit was still partially molten. Where withdrawal has not occurred, fill sequences are flat lying and symmetrically distributed around the feeder structures (cinder cones and dykes). The filled Nindiri pit holds  $5 \times 10^7 \text{ m}^3$  of lava in a 215-m-thick sequence. Partial fill of Santiago pit with  $1 \times 10^7 \text{ m}^3$  of lava has filled the pit with a 110-m-thick lava sequence, of which ~50% has been consumed by formation of a secondary pit. Altogether,  $6.4 \times 10^7 \text{ m}^3$  of lava was erupted into Nindiri and Santiago during 1525–1965, with 94% of this volume remaining pit-contained; the remainder forms a north flank lava flow field. Pit development and filling is a dynamic and ephemeral process, having short-lived effects on volcano morphology, where pits develop and fill over hours-to-centuries. However, pits play an important role in

shaping an edifice, representing lava sinks and controlling whether lavas are trapped or able to spread onto the flanks.

**Keywords** Pit craters · Lava lakes · Lava units · Masaya

## Introduction

Pit craters are circular to ellipsoid depressions with flat floors and steep to perpendicular walls (Stearns and Clark 1930; Wentworth and Macdonald 1953; Rittmann 1962). Pits craters are common on basaltic volcanoes including Kilauea (Walker 1988), Mauna Loa (Stearns and Clark 1930), Etna (Chester et al. 1985), Piton de la Fournaise (Carter et al. 2007) and Masaya (Roche et al. 2001) where they serve as natural depressions in which lava can become entrapped and pond. Lava flow activity in a pit crater is limited to the period of the eruption during which time a lava body becomes established within the pit. At the end of the eruption, the lava body will still be molten, but termination of supply will cause the lava lake to gradually cool, so that convection dies out and the lava lake eventually solidifies. Such lakes are termed “inactive lava lakes” by Swanson et al. (1979). In contrast, an “active lava lake” (Swanson et al. 1979) is rooted to an active conduit and remains active (molten and convecting) for decades-to-centuries. To form an inactive lava lake, lava can be erupted directly into the pit from vents opening on the pit floor or walls, or it can be filled by lava flows from external vents that cascade into the pit. Such pit-filling lavas are exposed in the walls of Santiago and San Pedro pit craters (Masaya, Nicaragua). Cutting of (older pit-filling) lavas by the two pit craters has provided a section through the crater-filling sequences, allowing reconstruction of the filling processes. In addition, the sequences show evidence of subsidence

---

Editorial responsibility: J McPhie

---

A. J. L. Harris (✉)  
HIGP/SOEST, University of Hawaii,  
1680 East-West Road,  
Honolulu, HI 96822, USA  
e-mail: harris@higp.hawaii.edu

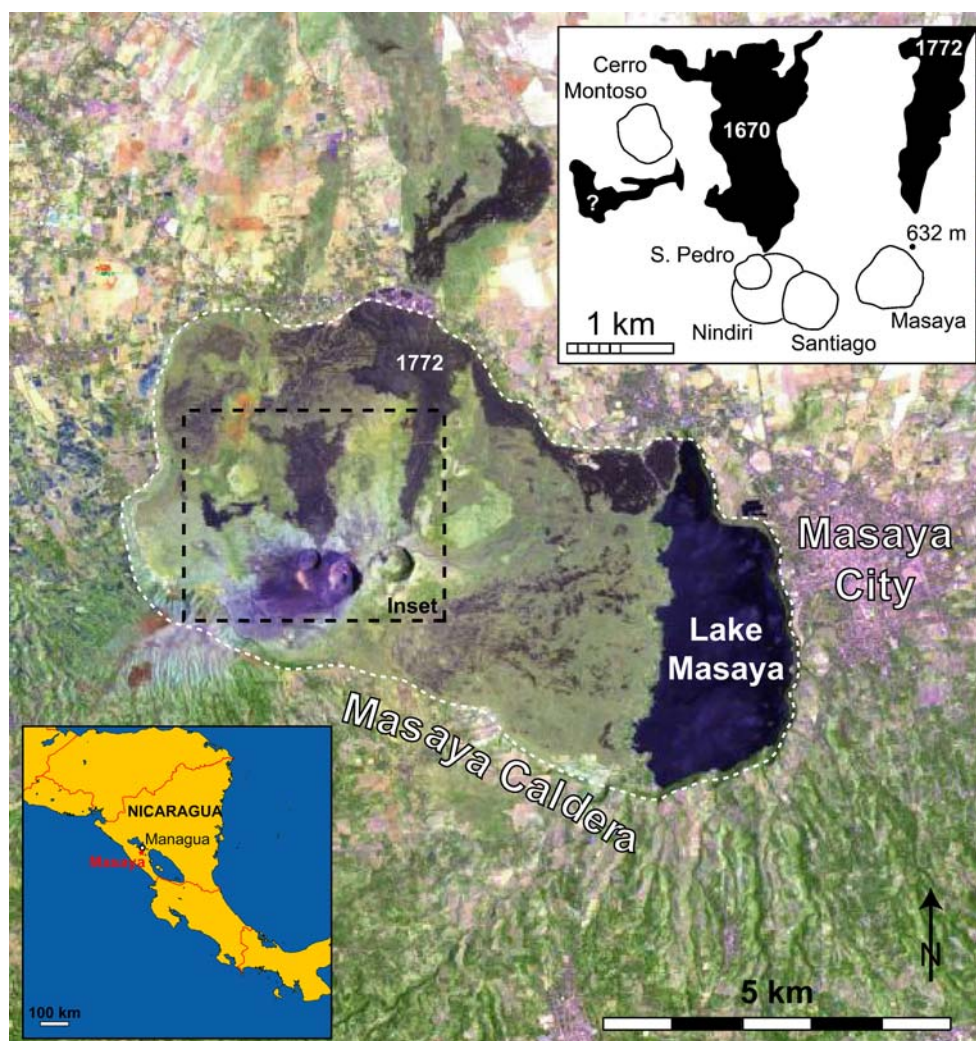
following lava withdrawal. Here, I describe and map these sequences to determine the emplacement styles and morphologies that characterize lavas erupting into, and ponding within, pit craters. In doing so, I refine the chronology of the recent effusive activity at Masaya.

### Pit craters and historic activity at Masaya

Masaya is a basaltic shield hosting a 11×6 km caldera within which a complex of lavas and cinder cones has developed centred on Masaya and Nindiri cones (Fig. 1). These cones are cut by four pit craters: Masaya, Nindiri, Santiago and San Pedro (Fig. 1). The Masaya pit is 650 by 620 m (Fig. 2). Maciejewski (1998) and Rymer et al. (1998) suggested that this pit formed sometime after 1525. It was last active in 1772 when a lava flow issued from the north-eastern flank of the cone (Fig. 1). Nindiri pit is 690 by 620 m (Fig. 2). Accounts by Oviedo (1855) indicate that, in

1525, it was 216 m deep and contained an active lava lake. The lake was absent in 1570, but may have been active intermittently during 1570–1670 to form a sequence of lava flows that ponded within Nindiri (McBirney 1956). These lavas eventually filled Nindiri and overflow in 1670 (Maciejewski 1998) emplaced a lava flow field on the northern flank (Fig. 1). Santiago and San Pedro pits subsequently opened, cutting and exposing the sequence of lavas erupted into Nindiri (Fig. 2). Maciejewski (1998) and Rymer et al. (1998), from observations in Montessus de Ballore (1888), dated formation of San Pedro and Santiago at 1858–59, although Stoiber et al. (1986) gave an earlier date of 1850–53 for Santiago. Santiago has subsequently been the main site of activity at Masaya (McBirney 1956; Rymer et al. 1998). Activity is characterised by degassing (e.g. Stoiber et al. 1986; Williams-Jones et al. 2003), punctuated by periods of spattering and lava lake activity; lava was last active on the floor of Santiago in 1946 and 1965 (McBirney 1956; Rymer et al. 1998). Santiago lava

**Fig. 1** ETM+ image of Masaya caldera. Outline of pit crater rims and historic lava flows (mapped using 15-m ETM+ panchromatic band) is *inset*. Flow field marked ? (*inset*) is of unknown date, but has a similar (young, unvegetated) surface to those of 1670 and 1772



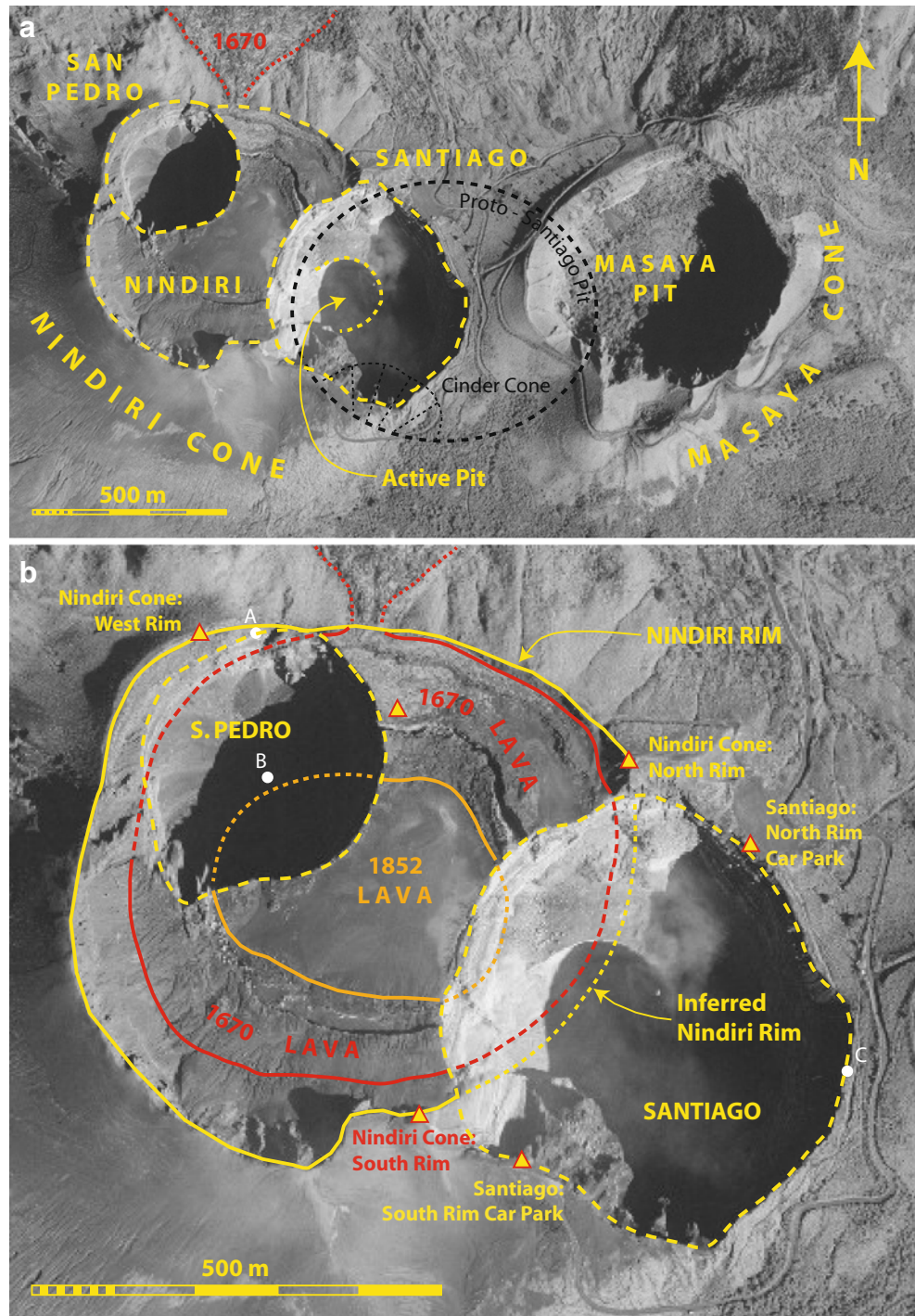
sampled in 1981 by Stoiber et al. (1986), along with analysis of 1772 lava (Williams 1983), show the lava to be basalt with 51–52 wt.% SiO<sub>2</sub> content, and Na<sub>2</sub>O + K<sub>2</sub>O of 4–5 wt.%, typical of recent Masaya compositions.

Methods

Pit floors and walls were mapped in March 2003 using a laser-range finder total station comprising a LaserTech

Impulse 200 XL fitted to a MapStar angle encoder. This instrument measures distances to an accuracy of 1 m and vertical/horizontal angles to 0.05°. In all, 3,760 control points were taken from six GPS-fixed survey points (Fig. 2b). Digital camera photo mosaics were also taken from each survey point. Stratigraphic logs supported by tape measure and compass-clinometer measurements were also made during February 2002 and March 2003. This approach allowed scaled mapping of all sequences and generation

**Fig. 2** **a** Aerial photo of San Pedro, Nindiri, Santiago and Masaya, giving: 1 spillway feeding Nindiri’s 1670 overflow (red), 2 approximate location of Proto-Santiago and cinder cone (black broken lines), and 3 active vent and pit (active pit). Because of the continuity of the lava flow packages around the Proto-Santiago cinder cone, the filled Proto-Santiago is here mapped as a single pit, rather than two separate pits as suggested by Maciejewski (1998) and Roche et al. (2001). **b** Nindiri, showing the extent of 1670 (red) and 1852 (orange) pit-filling lava. A–B–C marks Fig. 7 profile. Yellow-red triangles give location of main triangulation points used for the laser range finder survey



of cross sections plus thickness, area and volume data for each crater-filling unit. Aerial photographs, an Enhanced Thematic Mapper Plus (ETM+) image and two IKONOS images were also used to map and measure lava unit and pit areas. The panchromatic bands of ETM+ and IKONOS provide 15-m and 1-m data, respectively. Unless otherwise stated, dimensions are given from the laser-range finder survey.

### Santiago: pit and stratigraphy

The west wall of Santiago cuts the Nindiri pit as well as the northern and southern flanks of the Nindiri cone (Figs. 2 and 3a). The northern, southern and eastern walls of Santiago cut a sequence of flat-lying 'a'a lavas interrupted by a cinder cone (Fig. 3a).

#### Santiago pit and floor

The floor of Santiago is flat, has a broadly circular perimeter and dimensions of 460 by 490 m (Table 1), and is bounded by near vertical walls. The main pit is 205 m deep on the eastern side and 170 m on the southern and northern sides. The extra depth on the eastern side is due to Masaya cone tephra that occurs on the eastern rim (Fig. 4a). The main pit is flooded by pahoehoe erupted in 1965 (Figs. 4a,b and 5) and has undergone a series of filling and collapse events documented by Rymer et al. (1998) for 1986–97. Crater floor collapse has created a 220×260 m inner pit that contains a degassing vent. The inner pit cuts the 1948–65 sequence, exposing 110 m of pahoehoe fill to the north (Figs. 4a,b and 5); the southern and western sides are covered by talus (Figs. 3a and 4a,b).

#### Nindiri cone: northern and southern rim sequences

Santiago cuts the northern and southern rims of Nindiri cone, exposing three packages each of roughly equal thickness; the northern and southern rim packages have similar thickness and character [c.f. NC1–NC3 (Fig. 5) and SC1–SC3 (Fig. 6a)]. The lowermost package (NC1 and SC1) comprises yellow tephra at its eastern edge, and a mixture of breccia and tephra elsewhere. NC1 is cut by a narrow dyke that extends into, but not through, the middle package (NC2). NC2 and SC2 are sequences of thin 'a'a lavas and are overlain by the upper packages (NC3 and SC3) which are sequences of well-bedded tephra (Fig. 5). The entire sequence, especially the lava units of NC2, is cut to the east: the lava units on this eastern edge having near vertical edges and no marginal autobreccia. The sequences are also cut by the (now filled) Nindiri pit.

#### Santiago eastern and southern wall sequences

The eastern and southern wall sequences comprise flat lying 'a'a lavas. The two sequences are separated by a cinder cone exposed in the southern wall (Fig. 3a). The 170-m-thick eastern wall sequence can be split into six packages on the basis of lava unit thickness (EW1–EW6, Fig. 6b) and comprises alternating packages of thick and thin units (Table 2). The lower-most package (EW1) comprises two 20-m-thick 'a'a lavas with thick coherent cores. Above this EW2 is a 20-m-thick sequence of four thinner 'a'a lavas with well-developed top and basal autobreccia. EW3 comprises two thick 'a'a lavas which merge into a single unit towards the southern wall cone (Fig. 6b). A sequence of thin 'a'a lavas comprises EW4; up to five units can be identified, which pinch in and out along the exposure (Fig. 6b). EW5 comprises three thick 'a'a lavas and is followed by the sequence of four thin EW6 units. The sequence is capped by Masaya cone tephra that has a maximum thickness of 34 m (Table 2). All units onlap the southern wall cone (Fig. 6b) and can be traced around the crater to the north where they rest against the steep face of the Nindiri northern cone sequence (Fig. 5). The southern wall sequence can also be split into six packages of flat lying 'a'a. Each rests against the southern wall cone to the east and the steep face of the Nindiri southern cone sequence to the west (Fig. 6a). Above a coherent basal package (SW1), SW2 and SW3 comprise six thin and two thick 'a'a lavas, respectively. SW4 is a mix of black tephra and thin 'a'a lavas. SW5 is dominated by coherent lava that laps against the southern wall cone. The sequence is capped by a series of thin lavas overlying black tephra. Laser returns could not be obtained through the gas, making unit thickness measurement impossible. However, the sequence is 170 m thick, identical to the eastern wall sequence. All eastern and southern wall units can be linked to the southern wall cone. Lavas were fed by sill-to-dike like features that extended outwards from the cone centre (Fig. 6). The sill-to-dike like features have the form of broad "U" shapes. I thus interpret them as intrusions, rather than intra-cone lava lakes (crater-ponded lava would have a flat, rather than a concave, upper surface).

**Fig. 3 a** Aerial photo of Santiago delineating the main sequences exposed in the pit walls. *C–D* and *E–F* mark the ends Fig. 4a and b profiles, respectively. **b** Aerial photo of Nindiri showing surface features of the Nindiri lava fill of 1670 and 1852. *Dashed lines* indicate the projected exposures for sections now consumed by San Pedro or Santiago. The pit that opened in Nindiri's western sector to cut the 1852 unit is located (NP) as is the 1670 dyke. *G–H* and *I–J* mark the Fig. 4c and d transects

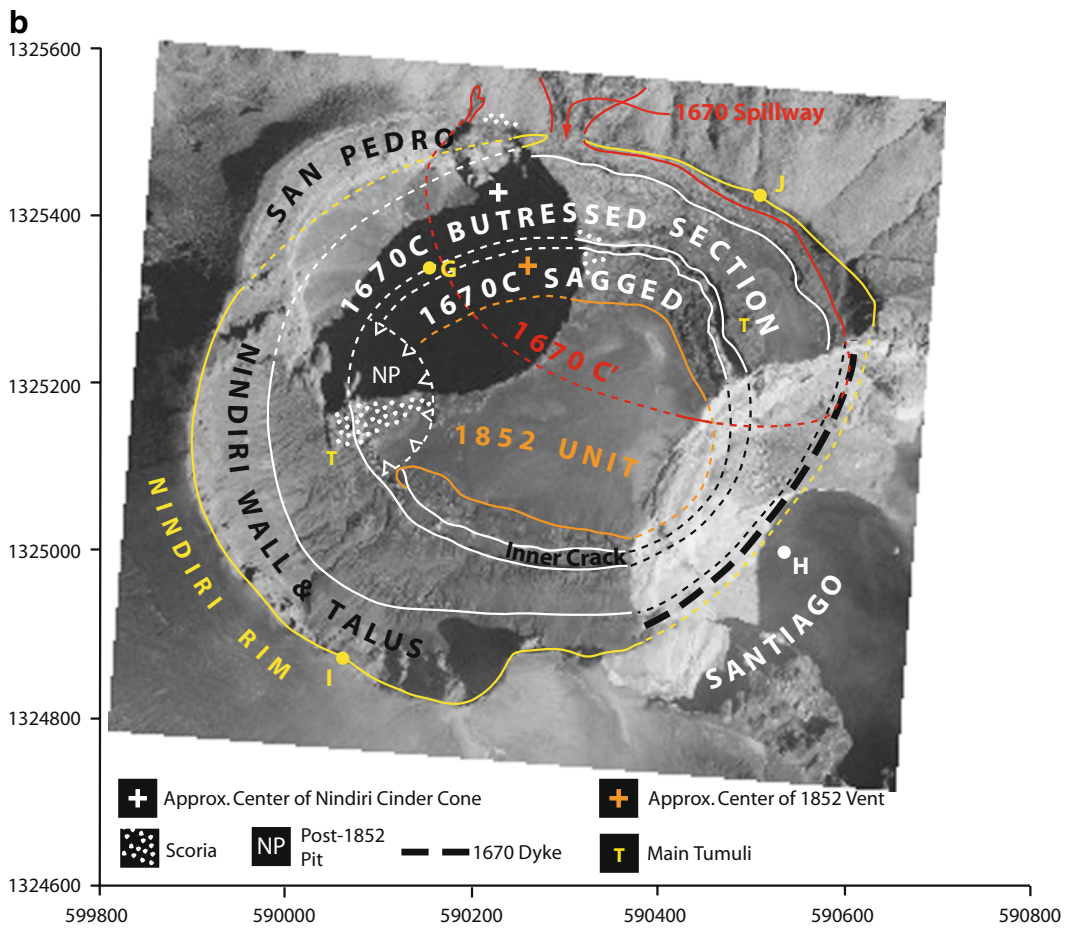
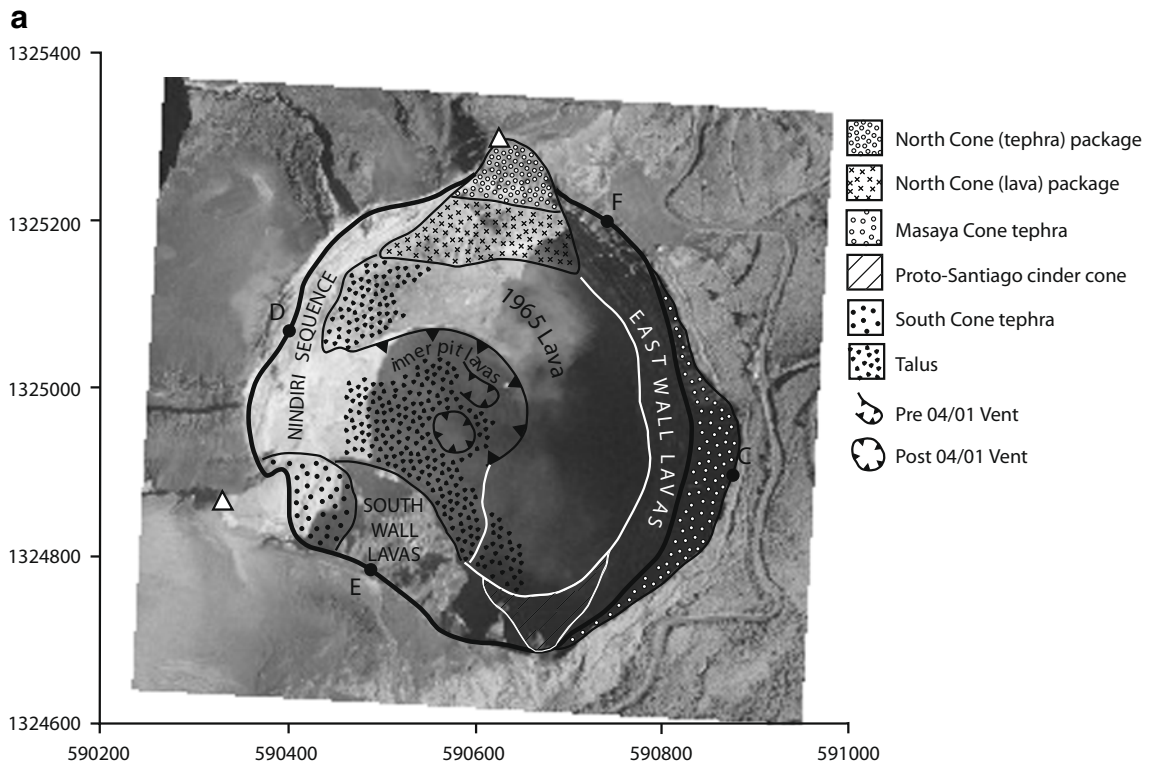


**Table 1** Pit dimensions and areas as of 2003

Pit	Diameter (m)		Area ( $\times 10^5 \text{ m}^2$ )		Depth (m)	Volume ( $\times 10^7 \text{ m}^3$ )
	N–S	E–W	Floor	Rim		
Proto-Santiago	760	760	4.50	4.50	170	7.65
Nindiri	580	560	2.49	2.49	216	5.38
Santiago	460	490	0.95	2.18	280	3.20
San Pedro	350	340	0.54	0.92	147	1.07

Volume = [(floor area + rim area)/2]  $\times$  depth. Proto-Santiago is assumed to be a circular, vertically sided pit. Dimensions and areas are IKONOS-based; depths are from laser range finder data. Nindiri floor area is not known, but following Oviedo (1855) the pit is assumed to be vertically-sided so that rim area  $\approx$  floor area. Santiago depth=2003 depth (170 m) + depth of 1946 and 1965 lava fill (110 m)=280 m.

**Santiago: formation and filling**

The Nindiri cone northern and southern rim sequences represent sections through the northern and southern flanks of Nindiri cone, respectively. This cone was cut first to the east by an older (now filled) pit (Proto-Santiago, Fig. 2) and then by Nindiri. Finally the sequence was cut by Santiago to expose the northern and southern flanks of Nindiri cone. Assuming a circular plan (Fig. 2), Proto-Santiago was  $\sim$ 760 m across (Table 1). Maciejewski (1998) suggested that there were two pits each containing the eastern and southern wall sequences, as is also implied by Fig. 9 of Roche et al. (2001). However, the identical heights of the eastern and southern wall sequences, their common linkage to the southern wall cone and the symmetry of each package around the cone, indicate that they ponded in a single pit fed by the same intra-pit cone. Filling of Proto-Santiago involved emplacement of 20 'a'a lavas. This

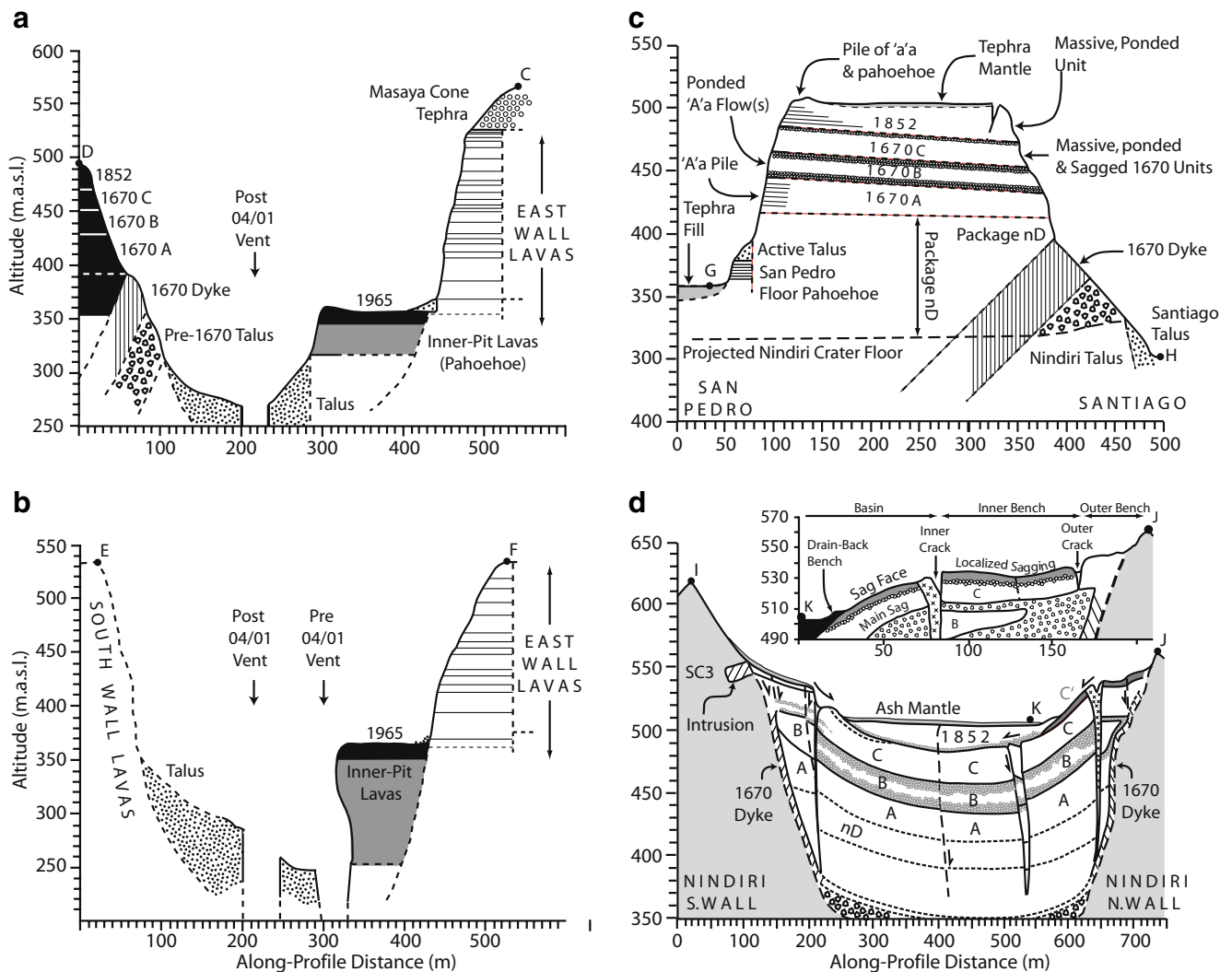
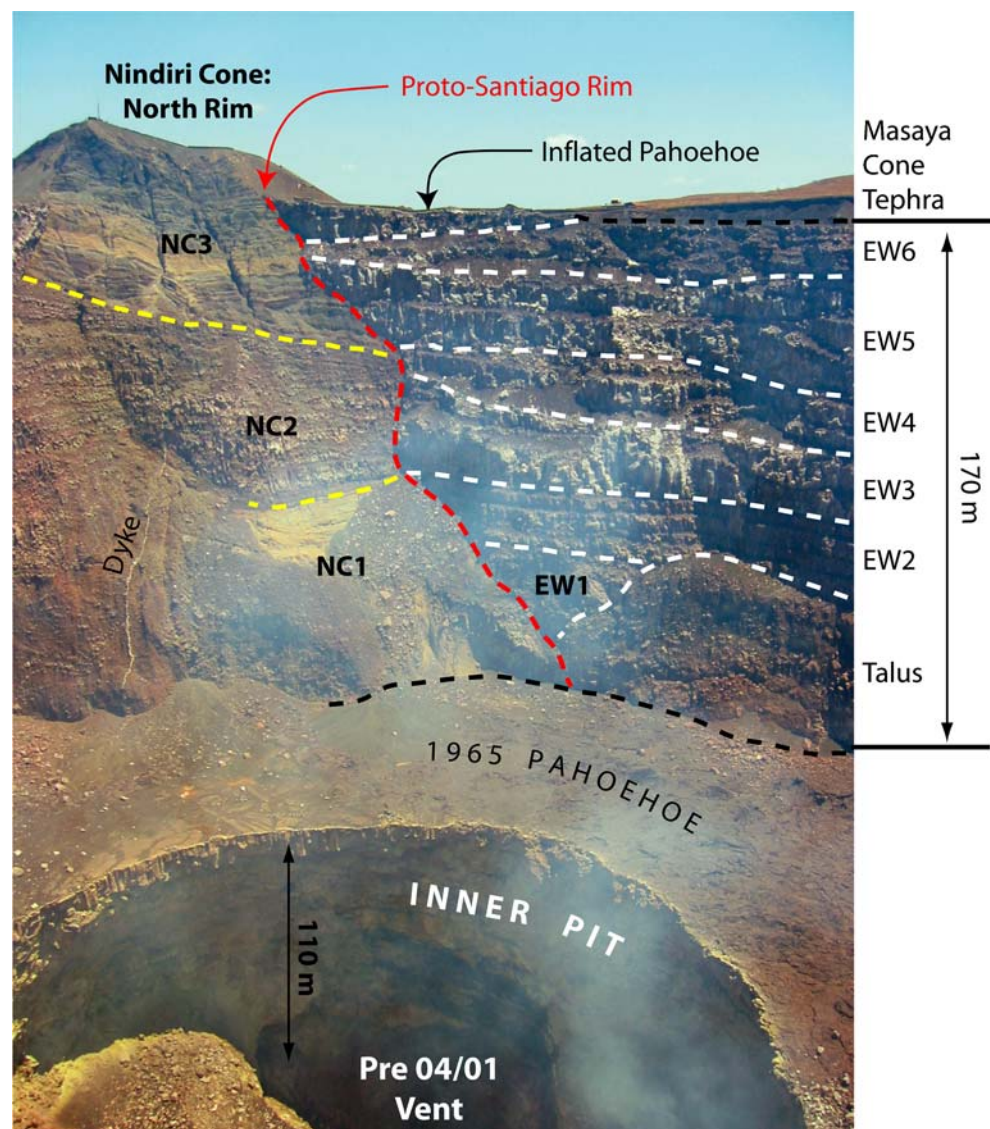


**Fig. 4** Santiago profiles: **a** west-east (D–C, Fig. 3a), **b** south–north (E–F, Fig. 3b), **c** west–east profile through Nindiri (line G–H, Fig. 3b), **d** south–north profile through Nindiri (line I–J, Fig. 3b). The portion marked K–J is enlarged as inset

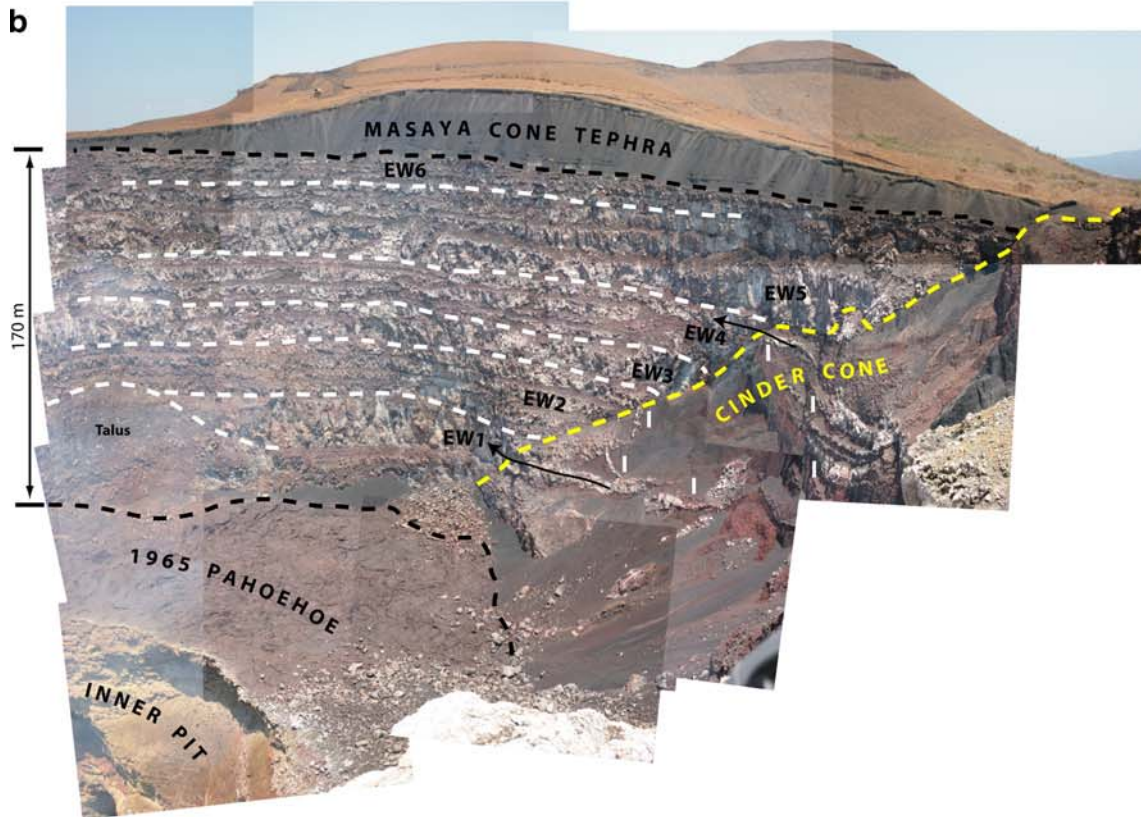
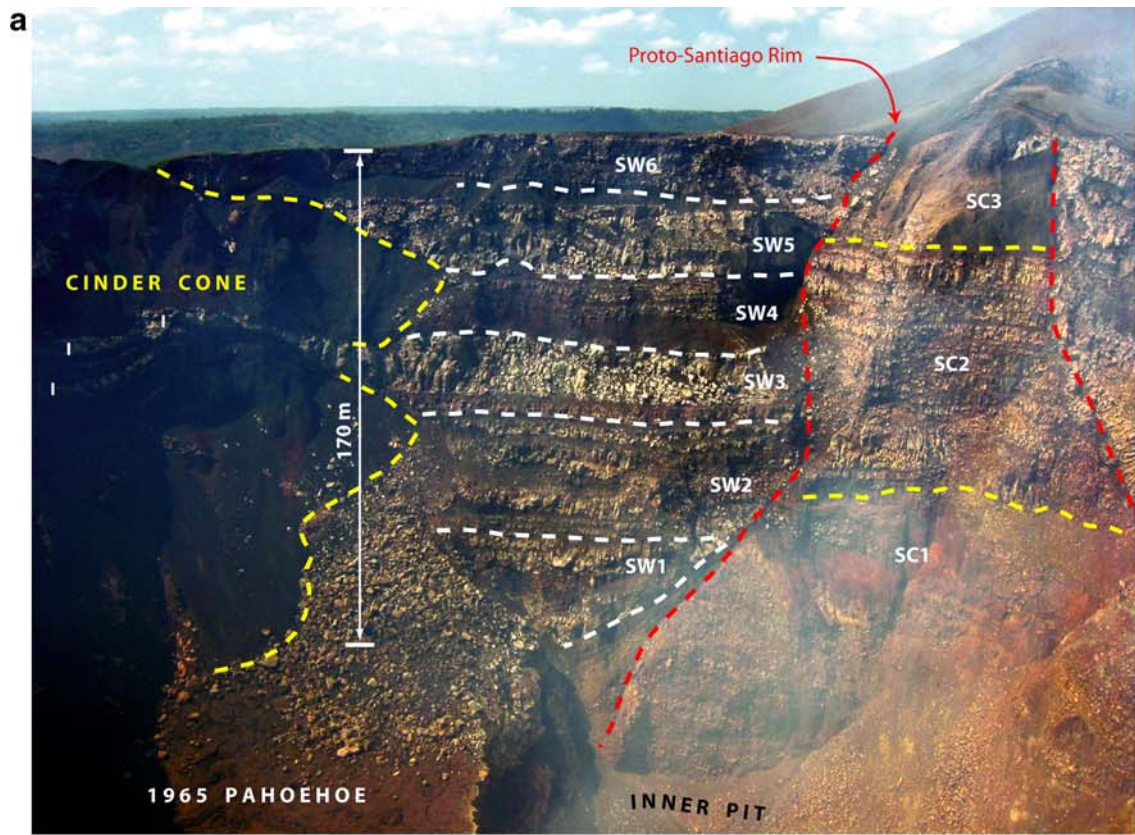
**Fig. 5** Northern floor and wall of Santiago showing inner pit, packages of the Nindiri's northern cone sequence and the eastern wall lavas



sequence comprises alternating packages of thick and thin lavas that filled the pit with a bulk lava volume of  $7.8 \times 10^7 \text{ m}^3$  (Table 2). Each lava flow retained its identity as a discrete cooling unit, having solidified before the next lava flow was superimposed. This means that sufficient time had to pass between each flow emplacement event to allow cooling (Walker 1972). All lavas can be traced to a cinder cone that built within the Proto-Santiago pit, banked up against its southern wall. The flat-lying nature of the eastern and southern wall units, as well as their symmetry around the cone and identical thickness around the entire section, suggest that they were entrapped in a flat-floored pit. As a result they progressively filled the pit while surrounding and burying the cone. Pit overflow likely emplaced the inflated pahoehoe of the southern flank of Santiago. Thus, although the effusive events that fed each of the 20 lava units that make up the Proto-Santiago fill sequence were characterised primarily by emplacement of 'a'a lavas, the final

(overflowing) event, at least, emplaced pahoehoe. A small lens of lava that pinches out beneath the northern rim car park is also inflated pahoehoe, as opposed to 'a'a which dominates the Proto-Santiago filling sequence below it (Fig. 5).

These pit-filling units were then cut by modern Santiago. As of 2003, eruption of pahoehoe (mostly during 1948 and 1965) had filled Santiago by at least 110 m. Given an IKONOS-derived crater floor area of  $95,000 \text{ m}^2$  (Table 1), the lavas have a minimum volume of  $10^7 \text{ m}^3$ . Post-1965 collapse has created an inner pit that increased in width from 80 m in 1986 (Rymer et al. 1998) to 260 m by 2003. As of 2001, the IKONOS-derived inner pit area was  $42,000 \text{ m}^2$  which, given a depth of 110 m, meant that  $\sim 0.5 \times 10^7 \text{ m}^3$  (or 50%) of the 1948–65 lava volume had been lost to collapse. The main pit depth of 170 m, along with the IKONOS-derived floor and rim areas (Table 1), give a main pit volume of  $2.7 \times 10^7 \text{ m}^3$ , to which the inner pit adds  $\sim 0.5 \times 10^7 \text{ m}^3$ .





◀ **Fig. 6 a** Southern floor and wall of Santiago showing the inner pit, the packages of Nindiri's southern cone, the southern wall lavas. The southern half of the Proto-Santiago cinder cone is also apparent, where intrusive (sill-to-dyke-like) bodies within the cone are marked "P". **b** Eastern floor and wall of Santiago showing the inner pit, eastern wall sequence and Masaya cone tephra. The northern half of the Proto-Santiago cinder cone is also apparent, where intrusive (sill-to-dyke-like) bodies within the cone are marked "P"

### The Nindiri lava lake sequence

Formation of Santiago and San Pedro exposed the ponded lavas that filled Nindiri (Fig. 7). The Santiago face of Nindiri exposes a section that is of a greater height (215 m), and less shattered, than the San Pedro section (147-m-high and heavily shattered). However, both sections reveal packages the contacts of which can be traced across Nindiri to crop out at approximately the same level (Fig. 7).

#### Nindiri lava lakes: the Santiago section

Five packages are apparent in the Santiago face of Nindiri: Nindiri talus, 1670 dyke, nD, 1670 lava and 1852 lava

(Fig. 8a). Of these the 1670 package can be split into three units: A, B and C (Fig. 8a; Table 3). The lower-most package (Nindiri talus) is an 85-m-thick layer of red (oxidised) talus. Following Maciejewski (1998), I assume that this is crater-floor talus that banked up against the eastern wall of Nindiri pit. This talus is cut near-vertically by Santiago. The talus base is at a depth of 215 m, identical to the pit depth of 216 m reported for (an empty) Nindiri by Oviedo (1855) in 1525, confirming that the sequence above the talus exposes the full thickness of Nindiri-filling units. Above the talus are two packages: (1) a 35-m-thick coherent unit with well-developed columnar joints (1670 dyke, Fig. 8a) followed by (2) a coherent, but shattered, 14-m-thick unit (nD, Fig. 8a). The upper portion of the section is dominated by a 59-m-thick package comprising three ~20-m-thick units with coherent cores and autobrecciated tops and bottoms (units 1670A–C). Autobreccia is best developed at the top and bottom of the middle unit (unit B). The uppermost unit (unit C) shows crude columnar joints, as would be expected in slow cooling of a thick crater-ponded flow (Peck and Minakami 1968). Where exposed in cracks on the northern side of Nindiri, a 1.5–1.7 m thick layer of autobreccia caps C. On the south side of Nindiri, C

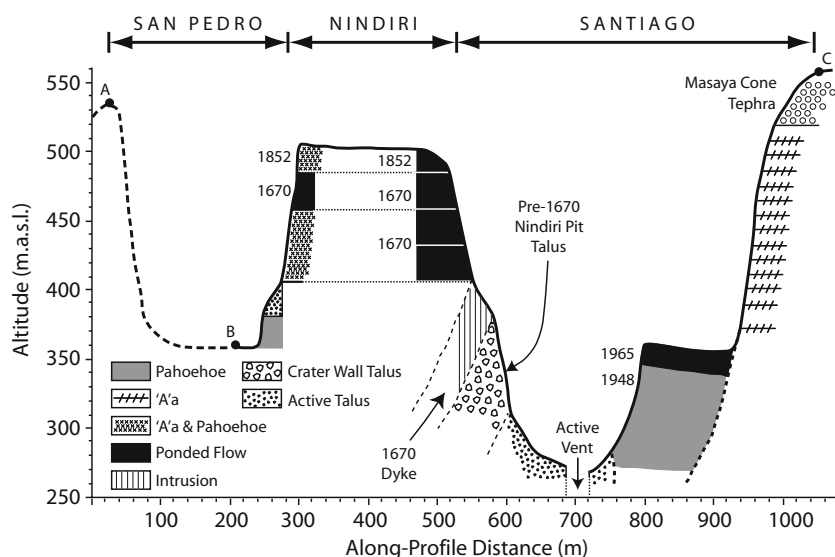
**Table 2** Santiago southern wall: package thickness and volume

Package	Unit	Unit no.	Contact elevation (m)	Unit thickness (m)	Volume ( $\times 10^6$ m <sup>3</sup> )	Package thickness (m)	Package volume ( $\times 10^6$ m <sup>3</sup> )
EW6	Masaya Cone Tephra		560	34			
	EW6: Lava Unit #4	20	526	4	1.81	16	7.3
	EW6: Lava Unit #3	19	522	4	1.81		
	EW6: Lava Unit #2	18	518	3	1.36		
	EW6: Lava Unit #1	17	515	5	2.27		
EW5	EW5: Lava Unit #3	16	510	12	5.44		
	EW5: Lava Unit #2	15	498	10	4.54		
	EW5: Lava Unit #1	14	488	11	4.99		
EW4	EW4: Lava Unit #5	13	477	2	9.07	25	11.3
	EW4: Lava Unit #4	12	475	8	3.63		
	EW4: Lava Unit #3	11	467	6	2.72		
	EW4: Lava Unit #2	10	461	6	2.72		
	EW4: Lava Unit #1	9	455	3	1.36		
EW3	EW3: Lava Unit #2	8	452	13	5.90	23	10.4
	EW3: Lava Unit #1	7	439	10	4.54		
EW2	EW2: Lava Unit #4	6	429	5	2.27	21	9.5
	EW2: Lava Unit #3	5	424	3	1.36		
	EW2: Lava Unit #2	4	421	9	4.08		
	EW2: Lava Unit #1	3	412	4	1.81		
EW1	EW1: Lava Unit #2	2	408	20	9.07	53 <sup>a</sup>	24.0 <sup>a</sup>
	EW1: Lava Unit #1	1	388	21	9.53		
	Talus		367	12			
	Crater Floor		355				
Total		20		205	72.1	171 <sup>a</sup>	77.6 <sup>a</sup>

Unit and package volumes assume ponded emplacement in a circular (Proto-Santiago) pit of radius 380 m

<sup>a</sup> Estimate excludes the Masaya cone tephra, but includes lowermost portion of EW1 buried by crater floor talus, so that EW1 thickness is 41+12 m=53 m.

**Fig. 7** West–east profile through San Pedro, Nindiri and Santiago (line A–B–C, Fig. 2)



has a variety of surface textures ranging from 'a'a to pahoehoe. A well-developed tumulus is also apparent on the surface of C in Nindiri's W sector (Fig. 3b). The pahoehoe of unit C contains cm-sized stretched vesicles and has a spiny surface, the stretched and broken vesicle walls forming the spines. The surface also displays ropes, slabs and bands of incipient 'a'a clast formation. This upper surface layer has a 15–25% phenocryst content and a vesicularity of 30–50%. However, where cracks expose C to depths of 20 m, a dense (vesicle-poor) core is apparent. This pattern is consistent with vesicularity profiles obtained for Alae lava lake (Kilauea) by Peck (1978) which show vesicularities of 20–40% in the uppermost 1.5 m declining to ~11% at a depth of 3 m.

On the northern side of the Santiago section, C is overlain by a fourth unit (C', Fig. 8a). C' has a maximum thickness of ~10 m near the northern Nindiri wall and pinches out towards the centre of the exposure (Fig. 8a). Where exposed in circumferential cracks, C' is present as a 1.7-m-thick layer of pahoehoe overlying the autobreccia surface of C. The surface of C' is dominated by spiny pahoehoe and contains several tumuli, including a prominent ~5-m-high tumulus in Nindiri's E sector (Fig. 3b). C' can be traced along the northern sector of Nindiri to a spillway that feeds the 1670 overflow (Fig. 3b). The centre of the section is capped by a coherent, lenticular, package (1852, Fig. 8a). This package overlies both C and C', with C' pinching out beneath the northern edge of the 1852 package (Fig. 8a). The 1852 package has a maximum thickness of 22 m at its centre and is covered by reworked tephra (Fig. 8a).

A dyke runs up the contact between Nindiri's wall and the sequence of pit-filling lavas (units A–C') on both the northern and southern sides of the Santiago exposure (1670 dyke, Figs. 8a and 3b). On the northern side it feeds C' and

on the southern side C. On the southern side it also intrudes Nindiri cone by a few meters (Fig. 4d). On both sides, it is 3–6 m wide and displays cross-dyke joints. The coherent, jointed package that overlies the Nindiri talus (1670 dyke, Fig. 8a) can be explained in terms of the same dyke cut at a steep angle by collapse of Santiago, revealing an apparent thickness much greater than the true thickness (Fig. 4c). The dyke does not crop-out in the western (San Pedro) exposure, implying that the dyke intruded the eastern side of a largely filled Nindiri pit along a semi-circular sector to feed units C and C' (Fig. 3b).

**Nindiri lava lakes: subsidence features, cracks, benches and drain back**

Where units A–C are buttressed by Nindiri's walls they are flat lying and pinch out towards the crater walls, resting against them (Fig. 8a). Buttressing of these units results in a ~100-m-wide bench that runs around the perimeter of Nindiri (1670C buttressed section, Fig. 3b). Where unsupported (towards the centre of Nindiri), all three units have subsided by 40 m and have broken into five main blocks (Figs. 8a and 4d). Subsidence has led to the opening of an inner circumferential crack ~100 m inside of the crater rim and roughly above the point of contact between Nindiri's preexisting pit wall and floor (inner crack, Figs. 3b and 4d). The inner crack runs around Nindiri's perimeter (Fig. 3b) and extends from the base of A to the top of C', opening upwards to a maximum width of 20 m (Figs. 8a and 4d). The crack is clean and displays columnar jointing; indicating, following Nichols (1939), brittle failure of solid lava. Subsidence of A–C has also caused unit C to flex, so that inside of the inner circumferential crack, C dips downwards (beneath the 1852 package) at an angle of 30°, and its upper surface is a ~35-m-wide sag face (Fig. 4d,

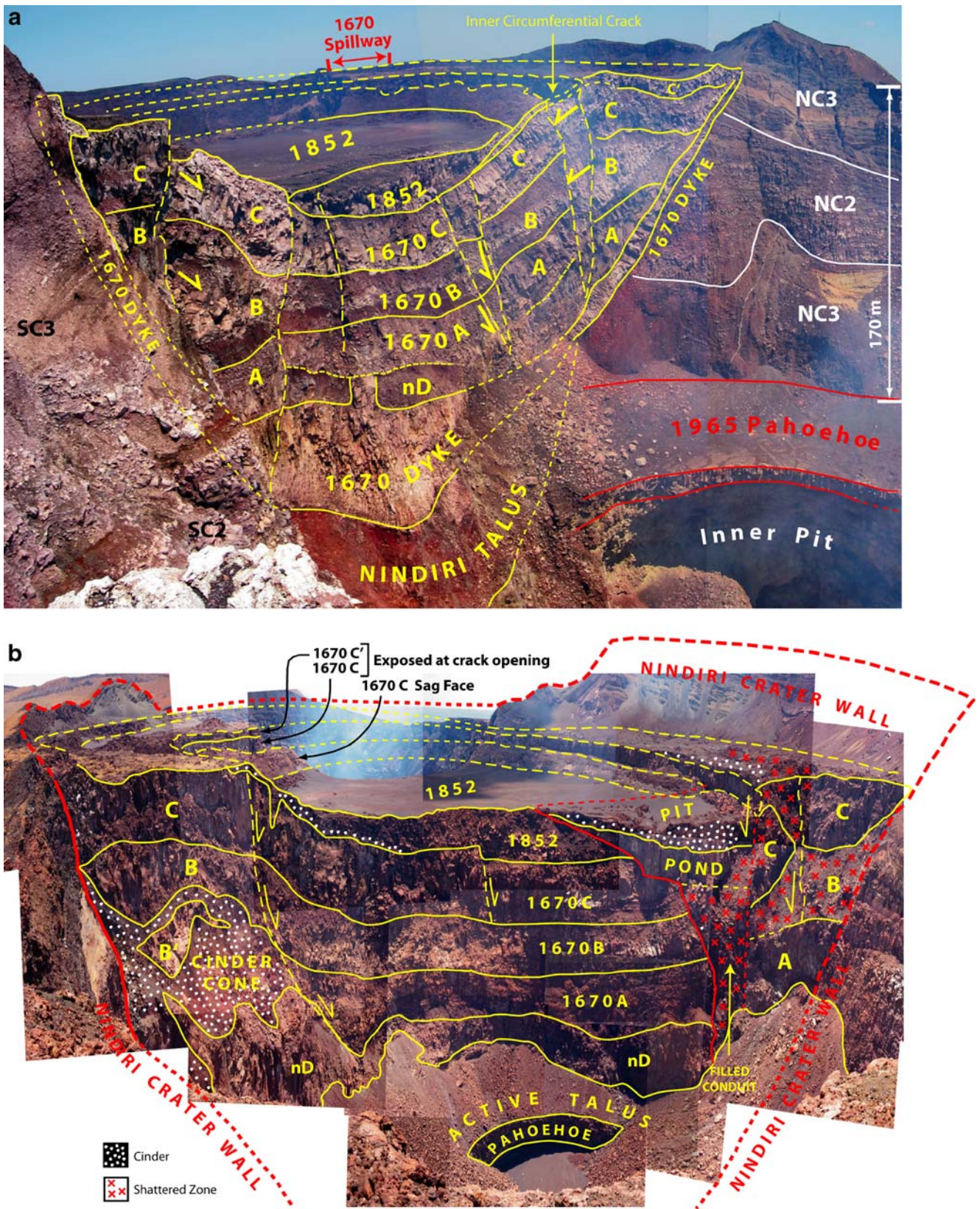


**Fig. 8** **a** Western floor and wall of Santiago showing the Nindiri-filling sequence. **b** Eastern floor and wall of San Pedro showing the Nindiri-filling sequence. For scale see Fig. 7—floor of San Pedro to top of 1852 package in section centre is 147 m

**Table 3** Nindiri eastern side (Santiago face) package thickness and volume

Package or unit	Package no.	Contact elevation (m)	Thickness (m)	Volume ( $\times 10^6$ m <sup>3</sup> )	Cooling time, Equation 1 (years)	Cooling time, Equation 2 (years)
1852 Lake	7	494	22	2.00	8.5	9.0
1670 C	6	472	20	4.98	7.0	7.4
1670 B	5	452	20	4.98	7.0	7.4
1670 A	4	432	19	4.73	6.3	6.7
nD <sup>a</sup>	3	413	14 (134)	33.37		
1670 Dyke	2	399	35			
Nindiri Talus	1	364	85			
Crater floor		279				
Total			215	50.07		

Lava volumes are bulk ( $V_{\text{bulk}}$ ) and use IKONOS-derived 1852 and 1670 unit areas ( $A$ ), these being  $0.91$  and  $2.49 \times 10^5$  m<sup>2</sup>, with the given unit or total thickness ( $h$ ), i.e.  $V_{\text{bulk}} = Ah$ . Cooling times are calculating using (1) Turcotte and Schubert (2002) and (2) Peck (1978).

<sup>a</sup>nD volume estimate assumes that the thickness of this package extends to the floor of the 215 m deep pit. The exposed thickness is given first and the full thickness in parentheses.

inset) surrounding the 1852 package (Fig. 3b). Extension of the crack through A–C', as well as the coupling of subsidence features between each of the units, indicates that all four units flexed and faulted together.

Between the inner circumferential crack and the Nindiri wall, C' has also sagged downwards by 8 m (Figs. 8a and 4d). Sagging has led to the opening of a 3-m-wide crack separated from Nindiri's northern wall by a 20-m-wide buttressed bench (Fig. 4d). Like the inner crack, the outer crack is parallel to the crater wall. The outer crack is 7.6 m deep and shows evidence of opening through solid and molten lava: the upper 3.4 m displays a clean break that narrows downward; suggestive of brittle failure. In contrast, the lowermost 4.2 m displays a concave surface on the crack's northern side so that it opens downwards into a cavern-like space. The concave face has a spiny texture with grooves and vertical stacks of decimetre-scale "sharks teeth" which have peeled away from the wall at their tops and are rooted to the wall at their bases. Grooves have been ascribed to solid lava being pulled across a soft surface (Nichols 1938; Nichols and Stearns 1939), and "sharks teeth" form where cracks open in lava that is still sticky (Nichols 1939). The lowermost 2 m of the crack comprises a bench with a convex upper surface overlain by flexed slabs (of sharks tooth form, but of meter scale) that are rooted to the crack wall and peel away from it. These features suggest the crack opened first by snapping of an upper solid (brittle) layer, and then propagated through a semi-molten layer. Within the semi-molten layer there are no signs of flow, indicative of high viscosity conditions (Nichols 1939). Groove orientation indicates a sense of movement that is downward and towards the crater centre. Such a scenario was noted at the subsiding Alae lake (Kilauea) where tension cracks penetrated through 3–5 m of brittle crust to bottom out in plastic lava (Swanson et al. 1972).

On the western side of Nindiri, 1852 lava has flowed into the inner crack to surround the sag face (Fig. 3b). On

the eastern side, drain back of 1852 lava is apparent from a 4–6-m-high bench of broken, foundered, slabs of surface (pahoehoe) crust. This bench is plastered to the lower section of the sag face. This feature is similar to the lava plaster (comprising broken slabs of pahoehoe) that became stranded on the sloping walls of Napau crater (Kilauea) following drain back of the fluid core of the 1968 lava that had become entrapped in Napau's pit (Jackson et al. 1975).

#### Nindiri lava lakes: the San Pedro section

The western side of the Nindiri sequence (as exposed in San Pedro) is more complex than the Santiago exposure due to shattering. However, the same three uppermost packages can be identified (nD, 1670 and 1852, Fig. 8b). The lowermost 22 m comprises a sequence of pahoehoe units which form a bench jutting out by 30 m from the base of the Nindiri face and which is mantled by talus (Fig. 8b). This lowermost sequence reveals filling of San Pedro by pahoehoe that was then cut by collapse of San Pedro's floor to form a shallow inner pit in the pahoehoe fill. Above the talus is a coherent package (nD, Fig. 8b), the top of which is level with the top of the nD exposure in the Santiago face (Fig. 4c). Above this, unit A of the 1670 package is shattered, but the tops and bottoms of at-least three 'a' lavas can be distinguished on the southern side of the section. Units B and C are also shattered, but are generally coherent in appearance (i.e. no flow units can be identified). All three units have thicknesses that are identical to those of A, B and C in the Santiago face (c.f. Tables 3 and 4). However, each unit crops out at a higher elevation in the San Pedro face, indicating east tilting of the sequence by  $\sim 2^\circ$  (Fig. 4c).

Units A–C show the same subsidence features as in the Santiago face (Fig. 8b). The upper (1852) package also thickens towards Nindiri's centre, consistent with ponding within the central bowl created by subsidence of A–C (Fig.

**Table 4** Nindiri western side (San Pedro exposure): package thickness and volume

Package or unit	Package or unit no.	Contact elevation (m)	Unit thickness (m)	Volume ( $\times 10^6$ m <sup>3</sup> )	Cooling time, Equation 1 (years)	Cooling time, Equation 1 (years)
1852 Lake	7	505	19	1.73	6.3	6.7
1670 C	6	486	20	4.98	7.0	7.4
1670 B	5	466	22	5.48	8.5	9.0
1670 A	4	444	20	4.98	7.0	7.4
ND <sup>a</sup>	3	424	37 (134)	33.37		
Active talus	2	387	44			
San Pedro pahoehoe	1	380	22			
Crater floor		358				
Total			147	50.57		

See Table 3 for volume and cooling time calculation.

<sup>a</sup>nD volume estimate assumes that the thickness of this package extends to the floor of the 215 m deep pit. The exposed thickness is given first and the full thickness in parentheses.

8b). However, although complicated by shattering, the 1852 package does not appear to be coherent as is the case in the Santiago face. Instead, single pahoehoe and 'a'a units can be distinguished, overlying a thin scoria bed. This scoria can also be found scattered across the surface of C close to the eastern rim of San Pedro, as well as interbedded with the 1852 units (Fig. 8b). This sequence appears to represent a pile of thin overflows building around a vent now lost due to collapse of San Pedro. Such a scenario is not unlike that encountered at Pauahi (Kilauea) during its 1973 eruption (Tilling et al. 1987) where a high effusion rate opening phase caused lava to pond in the eastern of the two pits that comprise Pauahi. During subsequent low effusion rate activity overflow of a syn-crater lava pond built a low shield surrounding the pond (Tilling et al. 1987).

To the north of the section, a cinder cone (overlying nD) is exposed (Fig. 8b). While unit A laps against the cone, B partially overlies and inter-fingers it, and C buries it. It thus appears to be the source for A and B, but not C. Cones at vents feeding lava flows can be found at the margins of Hawaiian pits, for example, the cone built during the 1959 eruption of Kilauea Iki (Richter et al. 1970). A smaller cone is also apparent banked up against the foot of the eastern wall of Keanakakoi (Kilauea) and is associated with the July 1974 eruption.

To the south, all packages (nD, 1670 and 1852) are truncated by an old conduit system. Package nD as well as units A, B and C are cut near-vertically by a breccia-filled structure. A, B and C can be traced either side of this structure, and C is also present within it (Fig. 8b). The structure is capped by a 15-m-thick coherent unit that thins over the 1852 lava (Fig. 8b). This coherent unit is, in turn, covered by 10 m of scoria that can also be found scattered across the surface of the 1670 bench in this sector of Nindiri (Fig. 8b). This structure is a filled conduit underlying a vent that

opened in the NW sector of Nindiri after emplacement of the 1852 lava (Fig. 3b). The vent had a similar geometry to the current Santiago vent, having a funnel-shaped upper section that opens into a broad pit (Fig. 8b). This vent was filled with ponded lava and then spatter before being cut by San Pedro. On the face of the 1670 crack above this vent, withdrawal of higher-standing lava has left a lava veneer. This veneer is similar to drain back veneers encountered on the walls of Hawaiian rifts in which lava ponded and then drained. This 5-m-high feature marks the highest stand of lava within the vent.

Nindiri overflow and the 1670 flow field: volume, viscosity and effusion rate

Lava from the uppermost fill unit (C') overflows Nindiri across a 45–50 m wide breach in the north rim (Fig. 3b). The spillway feeds the 1670 flow field, a compound field of slabby pahoehoe and 'a'a which contains complex, braided, channel networks. The IKONOS-derived flow field area is  $1.28 \times 10^6$  m<sup>2</sup>, having a width of 500–800 m, a N–S length of 2 km, and a longest centreline length (measured from the crater rim to the tip of the northwestern-most lava flow front) of 2.3 km (Fig. 1, inset). Shadows in the IKONOS image indicate a typical lava height around the margin of the 1670 flow field of 1–2 m, and levees and lobes within the field are 1–2 m higher. This is consistent with heights of 1–2 m measured at the margins of the proximal region of the flow field. A lava thickness of  $3 \pm 1$  m gives a bulk volume of  $3.85 \pm 1.28 \times 10^6$  m<sup>3</sup>. The spillway contains a 4.65-m-wide, 0.9-m-deep channel with overhanging rims, which have failed so that blocks of rim lie on the channel floor. The blocks have surfaces comprising annealed lava blebs elongated and tapered down-flow with drip-coated undersides, showing that a 10–40 cm thick roof was forming on the channel by annealing of lava blebs to the channel levee.

Given the channel depth and underlying slope (30°), Jeffreys (1925) equation can be used to estimate mean flow velocity if viscosity is known. For the glass composition for Santiago given by Stoiber et al. (1986), the method of Shaw (1972) gives a melt viscosity of 220 Pa s at 1,100°C. Following Marsh (1981), this value converts to a bulk viscosity (for a mixture with 20±5% phenocrysts) of 650±250 Pa s and yields a mean velocity of 3.8±1.5 m s<sup>-1</sup>. For a 4.65 m channel width, the bulk effusion rate is 18±7 m<sup>3</sup> s<sup>-1</sup>. This rate is a maximum because it assumes brim-full conditions, when below bank conditions are evident: a 0.45 m depth, evident from high stand marks on the channel walls, gives 0.35±0.15 m s<sup>-1</sup> and 1.7±0.7 m<sup>3</sup> s<sup>-1</sup>.

### Nindiri: unit cooling and subsidence

#### Unit cooling

Following Turcotte and Schubert (2002), the depth of the solidification boundary in a cooling lava ( $y_s$ , in millimetres) will increase with the square root of time ( $t$ , in seconds):

$$y_s = \lambda \sqrt{(\kappa t)} \quad (1)$$

$\lambda$  and  $\kappa$  being a dimensionless scaling value and lava thermal diffusivity (in mm s<sup>-1</sup>), respectively. For Hawaiian lava lakes Turcotte and Schubert (2002) calculate  $\lambda$  of 0.876. Thermal diffusivity can be calculated using lava thermal conductivity ( $k$ ), density ( $\rho$ ) and specific heat capacity ( $c_p$ ) in  $\kappa = k/\rho c_p$ . For Kilauea's Alae lava lake, Peck (1978) obtained (for a depth of 3–14 m)  $k$ ,  $\rho$  and  $c_p$  of 1.29 W m<sup>-1</sup> K<sup>-1</sup>, 2,670 kg m<sup>-3</sup> and 1,190 J kg<sup>-1</sup> K<sup>-1</sup>. These values yield  $\kappa$  of 0.6 mm<sup>2</sup> s<sup>-1</sup>. By estimating the time required for the solidification front to extend through each unit, Eq. 1 can be used to calculate maximum solidification time, giving 6–9 years for the uppermost units of the Nindiri sequence (Tables 3 and 4). The same relationship has been defined empirically using bore-hole-based temperature measurements at Hawaiian lava lakes. Peck et al. (1966) and Wright and Okamura (1977) both recorded downward migration of isotherms as a linear function of  $\sqrt{t}$  at Alae and Makaopuhi (Kilauea). From the Alae data Peck (1978) obtained:

$$y_c = 0.00132\sqrt{t} - 0.18 \quad (2)$$

$y_c$  being the thickness of the upper crust ( $y_c$ , in meters). This equation gives similar solidification times as the Turcotte and Schubert (2002) approach (Tables 3 and 4).

#### Subsidence and unit flexure

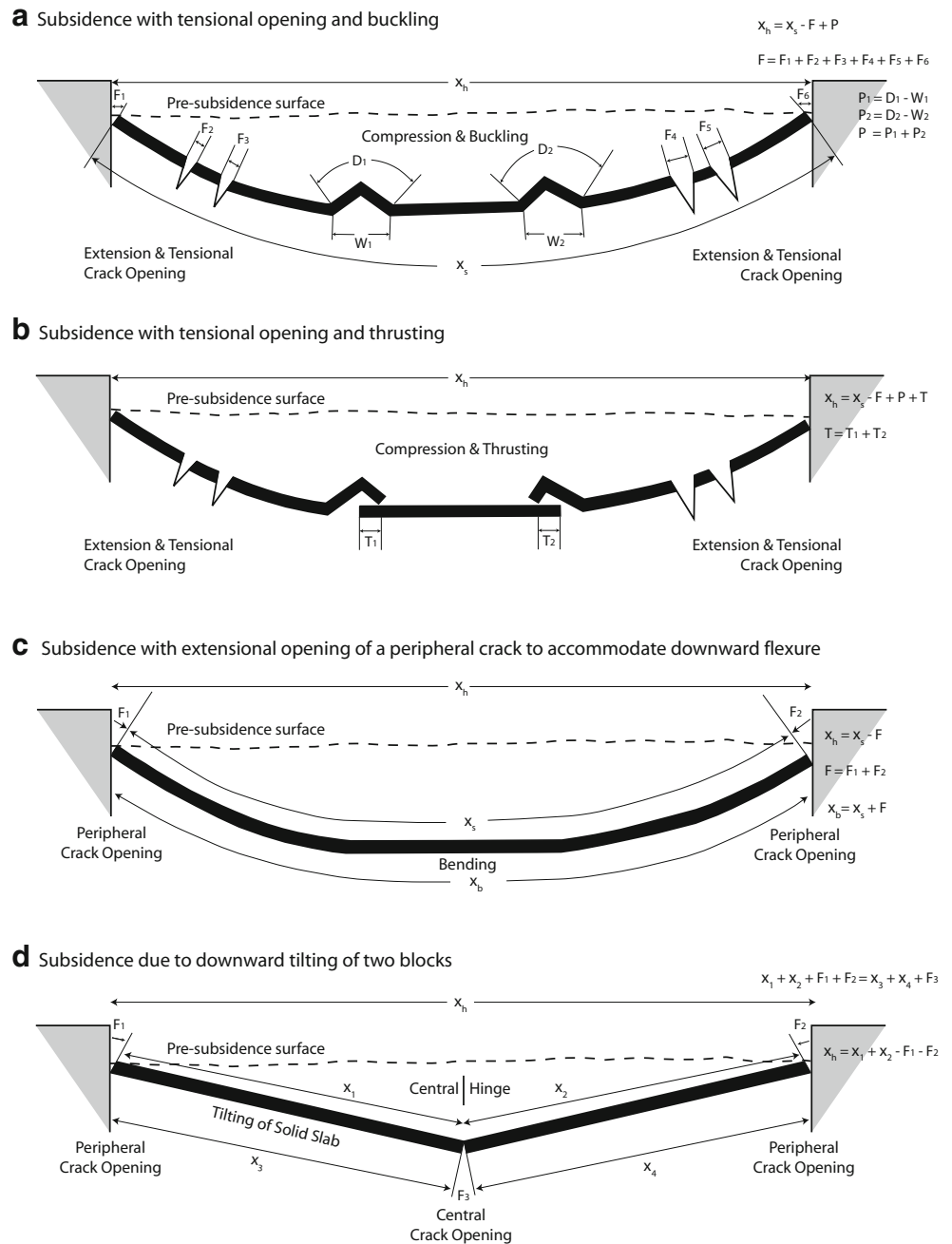
During subsidence of Kilauea's Alae lava lake, Swanson and Peterson (1972) observed thrust faults and pressure

ridges forming towards the centre of a subsidence bowl centred on the lake. Following the model of Swanson and Peterson (1972), in the absence of buckling due to compression, downward sagging of a lake surface and opening of surface tension cracks will mean that the sagged surface distance ( $x_s$ ) minus the total opening of tensional cracks ( $F$ ) should equal the horizontal (pre-sagged) surface distance ( $x_h$ ), i.e.  $x_s - F = x_h$  (Fig. 9a). In the case of subsidence at Alae, opening of tension cracks was too great, so that  $x_s - F$  was less than  $x_h$ . Thus thrusting must have occurred to account for the discrepancy (Swanson and Peterson 1972; Fig. 9b).

In the case of Nindiri's 1670C unit, measurements across transect I–J (Figs. 3b and 4d) give a pre-subsidence surface distance ( $x_h$ ) of 430 m. The circumferential tensional cracks bounding the subsidence bowl have widths of 10 and 20 m on the northern and southern sides, respectively, giving  $F$  of 30 m. The sagged surface length of ( $x_s$ ) along transect I–J is 460 m, meaning that  $x_s - F = 430$  m. This result is equal to  $x_h$  and implies that flexure can be accommodated by opening of circumferential tension cracks without compression and thrusting (Fig. 9c). In addition, the length of the bottom surface of C ( $x_b$ ) is 490 m, so that  $x_b = x_s + F$  (=460+30=490 m). These relationships are consistent with flexure of C to form a central subsidence bowl (Fig. 9c) bounded by an upward opening "mixed-mode fissure" which has both an opening and faulting component (Roche et al. 2001). Flexure of unit C is confirmed by laser ranger-finder measurements of the northern sag face that show a dip declining from 31° across the upper 17 m of the face to 28.5° in the lower 12 m so that it has a concave form.

In the Nindiri section the lava lake has also broken into a series of blocks (Fig. 8a). If these blocks toppled towards the centre of the pit, they should hinge along a line roughly central to the pit, so that a central hinge with compression at the top of the units and opening/extension at their bases (to match opening along the circumferential tensional cracks) should be evident (Fig. 9d). However, no such feature is apparent. Instead a series of faults are evident (Roche et al. 2001). Roche et al. (2001) determined that coherent piston collapse involves a scenario where the thickness/width ratio for the subsiding roof is less than or equal to 1. Given the thickness units A–C (~60 m) and width of the subsidence bowl (185 m) the roof thickness/width ratio would have been 0.3. The experimental results of Roche et al. (2000, 2001) showed that such subsidence will be accommodated by down-flexure, opening of a fracture at the limit of the depression, inward tilting of blocks and development of reverse faults. Roche et al. (2001) also showed that this scenario fits the structural features of Nindiri perfectly. Kaven and Martel (2007) concluded that, as a blind normal fault propagates toward the surface, the surface is flexed so that a monocline

**Fig. 9** Lava lake subsidence geometries for four scenarios involving: **a** opening of tensional cracks with central compression and buckling (Swanson and Peterson 1972); **b** opening of tensional cracks with central compression and thrusting (Swanson and Peterson 1972)—Alac case; **c** opening of circumferential tensional cracks and flexure with no buckling or thrusting—Masaya 1670 case (Roche et al. 2000, 2001); and **d** tilting of two blocks



develops and footwall fissures progressively widen and deepen. Buckles next develop on the hanging wall near the base of the scarp and cavities grow within the monocline. If the monocline does not collapse, then the limb of the monocline becomes progressively steeper as the fault tip nears the surface (Martel and Langley 2006; Kaven and Martel 2007). Both the field observations of such normal faults opening in basalt on Kilauea (Martel and Langley 2006) and experimental results (Holland et al. 2006) show similar structures (flexed surfaces and dilatant fractures) to those observed at Nindiri.

Subsidence bowl formation and timing of subsidence events

Following the eruption of A–C’ lava, withdrawal resulted in subsidence. The coupled behaviour of A–C’ shows that they subsided together, indicating that subsidence did not begin until after the final unit (C’) had been erupted. Subsidence resulted in brittle failure of the surface crust of C’ and opening of a circumferential tension crack that extended into molten lava (Fig. 9c). That the circumferential crack opened first through brittle crust and then through

a still molten layer indicates that crack opening was active when C' was still partially molten. This observation places a time limit on the onset of subsidence: it had to begin before the solidification front had reached a depth greater than 3.4 m. This, following Eq. 1, implies that fracturing occurred 75 days after the surface of C' began to cool. Thus, withdrawal of magma from the shallow system to cause the onset of subsidence and faulting likely occurred within 75 days of the eruption ending. Unbuttressed sections of Nindiri's 1670 package then flexed, bending downwards as fractures propagated upwards (Roche et al. 2000, 2001; Holland et al. 2006; Martel and Langley 2006; Kaven and Martel 2007) to form a central subsidence bowl bounded by circumferential cracks, the bowl having an IKONOS-derived radius of 185 m and area of  $30 \times 10^4 \text{ m}^2$ . The dip of the units to the east (Fig. 4c) also indicates that they became tilted downwards in this direction during subsidence. The resulting surface structure (Fig. 3b) is similar to the subsidence bowl encircled by tension cracks that formed over Kilauea's Alae lake during lava withdrawal in 1970 and 1971 (Swanson and Peterson 1972; Swanson et al. 1972). It also resembles features formed in 1932 across the surface of a subsiding lake within Kilauea's Halemaumau pit (Jaggard 1947, p. 190).

#### The 1852 lava: emplacement, cooling and timing of San Pedro–Santiago collapse

Montessus de Ballore (1888) noted lava effusion from Nindiri in July 1852, of which no trace can be found on the outer flank (McBirney 1956). Following Maciejewski (1998), this lava is assumed to have not escaped the crater, but instead ponded within the bowl formed by subsidence of A–C to form the uppermost package in the Nindiri fill sequence (1852, Fig. 8a). The 19–22-m-thick ponded portion of the 1852 lava would have taken 6–9 years to solidify (Tables 3 and 4). The 1852 lava, as exposed in Santiago, is cleanly cut and displays columnar joints (Fig. 8a). It was thus cut once it was solid. McBirney (1956) suggested that rumbling, detonations and ash emissions observed between November 1858 and March 1859 marked the formation of Santiago and San Pedro. The time between 1852 eruption and a 1859 collapse event ( $\approx 7$  years) would have been just sufficient to allow the 1852 lava to completely solidify (Tables 3 and 4). However, the 1850–53 date for the formation of Santiago given by Stoiber et al. (1986) would either have been before emplacement of the 1852 lava, or would have not given the lava time to solidify. After 1 year the unit would have had a  $\sim 7.5$  m thick brittle crust and a  $\sim 12.5$  m thick fluid interior capable of draining-out if exposed by pit crater collapse.

#### A chronology of pit crater formation and filling at Masaya

Based on the stratigraphy exposed in Santiago and San Pedro, the events responsible for formation and filling of Proto-Santiago, Nindiri and Santiago can be drawn up:

1. Nindiri cone was cut to the east by the Proto-Santiago pit. Proto-Santiago filled with sequences comprising thick ponded lavas and thinner 'a'a lavas fed by a cinder cone located in the pit's SW sector (Fig. 2a).
2. The filled Proto-Santiago pit was cut by Nindiri to the west. Nindiri was initially a steep-sided pit floored by talus now exposed in Santiago's western wall (Figs. 4d and 8a).
3. Vents opening on Nindiri's floor hosted active lava lakes. Repeated overflow built a sequence of pahoehoe and 'a'a flows which comprise the Nindiri floor lavas (nD; Fig. 8). These lavas filled the pit to a depth of 134 m (Tables 3 and 4; Fig. 4c) between 1570 and 1670 at a time-averaged discharge rate of  $1.6 \times 10^5 \text{ m}^3/\text{year}$  over 100 years.
4. Two thick, ponded, lava flows were emplaced within Nindiri (units 1670A and B, Figs. 4c and 8). These lavas were fed by a vent in Nindiri's NW sector over which a cinder cone formed (Fig. 3b). A dyke intruding the contact between Nindiri's talus and lava fill (package nD and units 1670A and B, Fig. 4c) fed the final two Nindiri-filling units (C and C'). C' overflowed Nindiri to the north in 1670 (Fig. 3b) to build a  $\sim 4 \times 10^6 \text{ m}^3$  lava flow field at peak effusion rates of  $18 \text{ m}^3 \text{ s}^{-1}$ . The four units (A, B, C and C') had a combined volume of  $1.5 \times 10^7 \text{ m}^3$  (Tables 3 and 4), increasing to  $1.9 \times 10^7 \text{ m}^3$  if the volume of the 1670 lava flow field is included.
5. Within 75 days of the end of the 1670 eruption, the sequence of Nindiri ponded units (A–C') subsided. A vent opening in Nindiri's NW sector (Fig. 3b) during June–July 1852 erupted scoria (now found on the 1670 bench) and a sequence of lava flows that formed a shield of pahoehoe and 'a'a around the vent. A 22-m-thick lake formed in the deeper eastern sector of the 1670 subsidence bowl. Ponding in the eastern sector was encouraged by a downward tilt of the 1670 units in this direction (Fig. 4c).
6. A second vent opened, sometime between 1852 and 1858, in Nindiri's W sector cutting the 1852 lava (NP, Fig. 3b). This vent was responsible for scoria on the 1670 bench in this sector, and filled with a localised (conduit contained) lava lake and scoria (Fig. 8b).
7. San Pedro and Santiago collapsed during 1858–59 to form two pits. San Pedro filled with 22 m of pahoehoe, within which a shallow pit opened. Santiago filled with 110 m of pahoehoe, during 1945 and 1965, within



which an inner pit opened hosting an active vent (Fig. 7).

## Discussion and conclusion

Lava flows erupting into Proto-Santiago, Nindiri and Santiago became entrapped by virtue of confinement in deep, steep-sided, flat-bottomed pits. Consequently, flows can only attain a maximum possible surface area defined by the pit limits to form thick, flat lying units (or inactive lava lakes) the thickness of which is controlled by geometric, rather than rheological, factors. Such an emplacement mechanism was recognised by Jaggar (1947, p. 103) who, under the perfectly descriptive title “Lava Lake a Confined Lava Flow”, stated that “a lava lake in a pit is nothing more than what would be if it were on a mountainside”. Following the classification applied by Walker (1972) to lava flows, two types of inactive lake (compound and simple) can be identified depending on whether they are divisible into flow units or not:

- Compound inactive lakes comprise sequences of multiple thin ‘a’ and pahoehoe flow units. These are fed at relatively low effusion rates, or by multiple (short-lived) overflows from vents active in the crater. As a result, each unit has sufficient time to cool before the next is emplaced, so that each unit maintains its identity to build a pile of thin flow units of limited extent. This scenario is similar to that observed at Pauahi (Kilauea) during 1973 (Tilling et al. 1987) and was likely the case in the construction of the compound sequence that comprises the Nindiri floor lavas (package nD), the thin-flow-packages of Proto-Santiago and the near-vent shield of the 1852 lava.
- Simple inactive lakes involve eruption of lava at high effusion rates, allowing no time for single cooling units to form. Instead, lava ponds and solidifies as a thick, coherent unit. The Hawaiian analogue is the rapid and high-effusion-rate filling of Kilauea Iki in 1959 (Richter et al. 1970). A similar emplacement scenario probably prevailed during the eruption of the thick-flow-packages of Proto-Santiago and the 1670 units of Nindiri. In the case of the 1852 lava, the eastward sloping crater floor resulting from tilting of the underlying units facilitated ponding in the lower-lying (eastern) portion of the 1670 subsidence bowl and formation of a simple, inactive lava lake in this location.

Vent structures include dykes, scoria cones and secondary pits. These sources not only feed syn-crater flow, but also contribute to pit fill. Withdrawal of magma by drain back down these feeding conduits and from the shallow

system will cause subsidence, as observed at Hawaiian lava lakes by Jaggar (1947), Swanson and Peterson (1972), Swanson et al. (1972) and Wright and Okamura (1977). Thick, solidified units are capable of deformation so that they flex downwards over unbuttressed portions of the lake as faults propagate upwards (Roche et al. 2000, 2001). When coupled with buttressing by the pit walls, a characteristic series of features results comprising circumferential benches, tension cracks and flexed surfaces surrounding a central subsidence bowl. These features are apparent in Nindiri’s units, where surface structures resemble those of Kilauea’s subsided lakes in Halemaumau and Alae (Jaggar 1947; Swanson and Peterson 1972; Swanson et al. 1972). Lavas that do not drain back remain flat lying, as is the case for the Proto-Santiago filling lavas.

Eruption of lavas into pit craters can be a significant sink for the erupted flux at an active volcano. Pit craters on Masaya represent a potential sink for  $17 \times 10^7 \text{ m}^3$  of lava (Table 1). Since 1525,  $6.4 \times 10^7 \text{ m}^3$  of lava has been erupted from Nindiri and Santiago. Of this, 94% ( $\sim 6 \times 10^7 \text{ m}^3$ ) has remained entrapped within the two pits (the remaining volume comprising the 1670 over-flow). This consideration does not include the volume erupted from the Masaya pit, which includes the 1772 flow field that was erupted from a fissure opening on the northern flank of Masaya (Fig. 1). Defining, mapping and measuring the volumes of pit-contained lava thus not only contributes to an assessment of the mass budget of a volcano or eruption (e.g. Swanson et al. 1979), but also aids in understanding eruption, drain back and edifice construction processes.

Pit development and filling is a dynamic and ephemeral process, often having short-lived effects on volcano morphology. Pits (from the crater- to caldera-scale) may develop and fill over time scales of hours-to-centuries (e.g. Dutton 1884; Dana 1891; Brigham 1909; Hitchcock 1909; Richter et al. 1970; Swanson et al. 1972; Walker 1988; Rymer et al. 1998). However, cycles of pit development and filling are important components of the evolution of an active basaltic edifice. Filling, and then emptying, of a summit crater or caldera can determine whether lavas are contained or free to extend onto the volcano flanks. Near-continuous summit overflow from a filled Kilauea caldera during 1290–1470, for example, built a series of summit shields (Holcomb 1987) and a  $5.2 \text{ km}^3$  lava flow field that extended to the coast (Clague et al. 1999). At Masaya, emplacement of lava flows on the edifice flank was only possible in 1670 once Nindiri’s pit had been filled, a process that took  $\sim 145$  years (1525–1670) and was followed (in 1859) by a new cycle of pit formation. Cycles of pit formation and filling are key processes at active basaltic volcanoes, determining vent location and defining whether lavas become entrapped and ponded, or are able to

flow freely (unimpeded by pit topography) onto the volcano flanks.

**Acknowledgements** Field work was supported by NASA grant NAG5-10640. ETM+ data were purchased through NAG5-10640 and IKONOS was provided through NASA's Science Data Purchase Program. Aerial photo's are courtesy INETER (Nicaragua) and made available by Glyn Williams-Jones. This manuscript benefited greatly from the reviews of Ben van Wyk de Vries and Glyn Williams-Jones, the excellent editorial handling of Jocelyn McPhie, an informal review by Lucia Gurioli, and discussions with Steve Martel and Don Swanson.

## References

- Brigham WT (1909) The volcanoes of Kilauea and Mauna Loa. *Memoirs of the Bernice Pauahi Bishop Museum* 2(4):1–608
- Carter A, van Wyk de Vries B, Kelfoun K, Bachèlery P, Briole P (2007) Pits, rifts and slumps: the summit structure of Piton de la Fournaise. *Bull Volcanol* 69:741–756
- Chester DK, Duncan AM, Guest JE, Kilburn CRJ (1985) Mount Etna: the anatomy of a volcano. Chapman & Hall, London
- Clague DA, Hagstrum JT, Champion DE, Beeson MH (1999) Kilauea summit overflows: their ages and distribution in the Puna District, Hawai'i. *Bull Volcanol* 61:363–381
- Dana JD (1891) Characteristics of volcanoes. Dodd, Mead and Company, New York
- de Oviedo y Valdes GF (1855) General and natural history of the Indias. Jose de los Rios, Madrid, Part 3 4:70–92
- Dutton CE (1884) Hawaiian volcanoes. 4th Annual Report of the US Geol Surv, pp 75–219
- Hitchcock CH (1909) Hawaii and its volcanoes. The Hawaiian Gazette Company, Honolulu
- Holcomb RT (1987) Eruptive history and long-term behavior of Kilauea volcano. *US Geol Surv Prof Pap* 1350:261–350
- Holland M, Urai JL, Martel S (2006) The internal structure of fault zones in basaltic sequences. *Earth Planet Sci Lett* 248:286–300
- Jackson DB, Swanson DA, Koyanagi RY, Wright TL (1975) The August and October 1968 East Rift eruptions of Kilauea Volcano, Hawaii. *US Geol Surv Prof Pap* 890:1–33
- Jaggard TA (1947) Origin and development of craters. *Geol Soc Am Mem* 21:1–508
- Jeffreys H (1925) Flow of water in an inclined channel of rectangular section. *Philos Mag J Sci* 49:793–807
- Kaven JO, Martel SJ (2007) Growth of surface-breaching normal faults as a three-dimensional fracturing process. *J Struct Geol* 29:1463–1476
- Maciejewski AJH (1998) Remote measurements of volcanic gases: applications of open-path Fourier transform infrared-spectroscopy (OP-FTIR) and correlation spectroscopy (COSPEC). PhD thesis, The Open University, Milton Keynes
- Marsh BD (1981) On the crystallinity, probability of occurrence, and rheology of lava and magma. *Contrib Mineral Petrol* 78:85–98
- Martel SJ, Langley JS (2006) Propagation of normal faults to the surface in basalt, Koae fault system, Hawaii. *J Struct Geol* 28:2123–2143
- McBirney AR (1956) The Nicaraguan volcano Masaya and its caldera. *EOS Trans Am Geophys Union* 37(1):83–96
- Montessus de Ballore F (1888) Tremblements de terre et eruptions volcaniques en center americque depuis la coquette espagnole jusqu'a nos jours. Societe Sciences Naturelles De Saoreet-Loire, Dijon, p 293
- Nichols RL (1938) Grooved lava. *J Geol* 46:601–614
- Nichols RL (1939) Surficial banding and shark's-tooth projections in the cracks of basaltic lava. *Am J Sci* 237:188–194
- Nichols RL, Stearns CE (1939) Grooved lava in the cross-section of Big Craters, Idaho. *Am J Sci* 237:22–31
- Peck DL (1978) Cooling and vesiculation of Alae lava lake, Hawaii. *US Geol Surv Prof Pap* 935-B:1–59
- Peck DL, Minakami T (1968) The formation of columnar joints in the upper part of Kilauean lava lakes, Hawaii. *Geol Soc Am Bull* 79:1151–1166
- Peck DL, Wright TL, Moore JG (1966) Crystallization of tholeiitic basalt in Alae lava lake, Hawaii. *Bull Volcanol* 29:487–498
- Richter DH, Eaton JP, Murata KJ, Ault WU, Krivoy HL (1970) Chronological narrative of the 1959–60 eruption of Kilauea volcano, Hawaii. *US Geol Surv Prof Pap* 537-E:1–73
- Rittmann A (1962) Volcanoes and their activity. Wiley, New York
- Roche O, Druitt TH, Merle O (2000) Experimental study of caldera formation. *J Geophys Res* 105:395–416
- Roche O, van Wyk de Vries B, Druitt TH (2001) Sub-surface structures and collapse mechanisms of summit pit craters. *J Volcanol Geotherm Res* 105:1–18
- Rymer H, van Wyk de Vries B, Stix J, Williams-Jones G (1998) Pit crater structure and processes governing persistent activity at Masaya Volcano, Nicaragua. *Bull Volcanol* 59:345–355
- Shaw HR (1972) Viscosities of magmatic silicate liquids: an empirical method of prediction. *Am J Sci* 272:870–893
- Stearns HT, Clark WO (1930) Geology and water resources of the Kau district, Hawaii. *Water Supply Paper* 616:1–194
- Stoiber RE, Williams SN, Huebert BJ (1986) Sulfur and halogen gases at Masaya caldera complex, Nicaragua: total flux and variations with time. *J Geophys Res* 91:12215–12231
- Swanson DA, Peterson DW (1972) Partial draining of Alae lava lake and the resulting crustal subsidence. *USGS Prof Pap* 800-C:1–14
- Swanson DA, Duffield WA, Jackson DB, Peterson DW (1972) The complex filling of Alae crater, Kilauea volcano, Hawaii. *Bull Volcanol* 36:105–126
- Swanson DA, Duffield WA, Jackson DB, Peterson DW (1979) Chronological narrative of the 1969–71 Mauna Ulu eruption of Kilauea Volcano, Hawaii. *US Geol Surv Prof Pap* 1056:1–55
- Tilling RI, Christansen RL, Duffield WA, Endo ET, Holcomb RT, Koyanagi RY, Peterson DW, Unger JD (1987) The 1972–1974 Mauna Ulu eruption, Kilauea Volcano: an example of quasi-steady-state magma transfer. *US Geol Surv Prof Pap* 1350:405–469
- Turcotte DL, Schubert G (2002) *Geodynamics*. Cambridge University Press, Cambridge
- Walker GPL (1972) Compound and simple lava flows and flood basalts. *Bull Volcanol* 35:579–590
- Walker GPL (1988) Three Hawaiian calderas: an origin through loading by shallow intrusions? *J Volcanol Geotherm Res* 93:14773–14784
- Wentworth CK, Macdonald GA (1953) Structures and forms of basaltic rocks in Hawaii. *US Geol Surv Bull* 994:1–97
- Williams SN (1983) Plinian airfall deposits of basaltic composition. *Geology* 11:211–214
- Williams-Jones G, Rymer H, Rothery DA (2003) Gravity changes and passive SO<sub>2</sub> degassing at the Masaya caldera complex, Nicaragua. *J Volcanol Geotherm Res* 123:137–160
- Wright TL, Okamura RT (1977) Cooling and crystallization of tholeiitic basalt, 1965 Makaopuhi lava lake, Hawaii. *US Geol Surv Prof Pap* 1004:1–78